REPRODUCTION QUALITY NOTICE

This document is the best quality available. The copy furnished to DTIC contained pages that may have the following quality problems:

- Pages smaller or larger than normal.
- Pages with background color or light colored printing.
- Pages with small type or poor printing; and or
- Pages with continuous tone material or color photographs.

Due to various output media available these conditions may or may not cause poor legibility in the microfiche or hardcopy output you receive.

☐ If this block is checked, the copy furnished to DTIC contained pages with color printing, that when reproduced in Black and White, may change detail o1 the original copy.

NAVORD REPORT 6182

FC

MAGNUS MOMENT ON PURE CONES IN SUPERSONIC FLIGHT (U)

20 JANUARY 1959

U. S. NAVAL ORDNANCE LABORATORY

WHITE OAK, MARYLAND

MAGNUS MOMENT ON PURE CONES IN SUPERSONIC FLIGHT

by

John D. Nicolaides*

and

John J. Brady

ABSTRACT: By aeroballistic range techniques, the Magnus moment is measured on 20° ~~degree~~ pure cones at $M \approx 2$ ~~a supersonic Mach number of about 2~~. The results indicate that the Magnus moment may be critically dependent, in both size and sign, on the nature of the boundary layer (i.e., laminar, turbulent, or mixed).

The normal force and damping moment are also found to be significantly dependent on the nature of the boundary layer.

The characteristics of the boundary layers are revealed in the spark shadowgraphs of the aeroballistic range technique and its transient and sometimes chaotic character noted. Criteria for specifying the general nature of the boundary layer are evolved and used to correlate the coefficient data.

The experimental force and moment coefficients are compared with theoretical values obtained from various suggested physical models of the flow.

Future programs for furthering the investigations are suggested.

---

* Scientific Advisor for Astronautics, Bureau of Ordnance, Washington, D.C.

U. S. NAVAL ORDNANCE LABORATORY
WHITE OAK, MARYLAND

NAVORD Report 6183 20 January 1959

This report gives the results of tests carried out at the Naval Ordnance Laboratory to determine the Magnus moment on 20-degree spinning cones as requested by the Bureau of Ordnance under task number 803-767/73002/01040.

The authors wish to take this opportunity to thank Mrs. Jeanne B. Jusino for conducting the firings and Miss Amy Chamberlin for reducing the basic data.

MELL A. PETERSON
Captain, USN
Commander

Z. I. SLAWSKY
By direction

Contents

Illustrations

Contents (Cont'd)

MAGNUS MOMENT ON PURE CONES IN SUPERSONIC FLIGHT

INTRODUCTION

1. The Magnus force has historically been of importance in the flight of all types of ballistic missiles, from round shot to shells and from arrows to fin-stabilized rockets and bombs. It is essential to seek out its size and role early in the design stages of missiles. Failure to do so in the past has frequently resulted in serious flight difficulties, often uncovered in the final stages of developmental testing.

2. An experimental determination of the Magnus moment acting on a pure cone in supersonic flight was desired for two main reasons; first, as a guide for the development of a rational fluid theory for predicting this fundamental aeroballistic moment* and, second, for use in the equations of motion for determining dynamic stability and performance of conical shapes. This information might also have additional engineering applications (1) in determining the trajectories of modern long-range ballistic missiles which re-enter the earth's atmosphere, and (2) in evaluating the contribution of the nose component of conventional rolling ballistic and guided missiles.

3. The aeroballistic range was selected as a facility in which to conduct this investigation because of its demonstrated capability for measuring Magnus effects and its availability. Although supersonic wind-tunnel techniques for the measurement of Magnus force and moment have developed with spectacular success in recent years, at the time of this investigation (1956) none were capable of obtaining Magnus measurements on pure cones.

4. The selection of the aeroballistic range technique with its spark shadowgraph pictures proved most fortunate, as will be noted later, because of the additional capability of examining the nature of the boundary-layer flow on the models in flight.

Aeroballistic Range Techniques

5. The aeroballistic range technique (reference (a)) for the experimental determination of the static and dynamic fluid forcer and moments which act on missiles in flight, employs free-flight models launched from guns and consists in

* The pure circular cone was selected because of its simplicity as perhaps the most fundamental of supersonic lifting configurations and because a maximum chance seemed to be promised for the possible formulation of a fluid theory for Magnus effect.

accurately determining the six position coordinates during their flight from a series of spark shadowgraphs taken at prescribed stations along the model's trajectory.

6. The linear solution for the angle of attack and angle of sideslip is given by

$$\vec{\alpha} = \beta + i\alpha = K_1 e^{(\lambda_1 + i\omega_1)s} + K_2 e^{(\lambda_2 + i\omega_2)s} \qquad (1)$$

where

$$\lambda_{1,2} \approx \frac{3\pi\rho d^2}{4m}\left\{ C_{N_\alpha}(1 \mp \tau) + \frac{md^2}{2I}\left(C_{M_q} + C_{M_{\dot\alpha}}\right)(1 \pm \tau) \pm C_{M_{p\alpha}}\frac{md^2\tau}{I_x} + C_D\left(2 - \tau^2 \mp \tau\right) + C_{l_p}\frac{md^2}{2I_x}\left(\tau - \tau^2\right)\right\}$$

$$\omega_{1,2} \approx \frac{c}{d}\left\{\left(\frac{pd}{2V}\right)\frac{2I_x}{I}\left(1 \pm \frac{1}{\tau}\right)\right\}$$

$$\tau = \frac{1}{\sqrt{1 - \frac{1}{s}}} \qquad s = \frac{\left(\frac{pd}{2V}\right)^2\left(\frac{2I_x}{I}\right)^2}{8\left(\frac{md^2}{2I}\right)\left(\frac{\rho S d}{2m}\right)C_{M_\alpha}}$$

This equation is "fitted" to the aeroballistic range position data by the method of differential corrections (reference (b) and (c)).

7. The static and dynamic aerodynamic coefficients and their probable errors are determined from the constants of equation (1) and the probable error of fit (reference (b)).

Experimental Program

8. Eleven 20-degree spinning cones were fired in the Naval Ordnance Laboratory's Pressurized Ballistics Range (Figure 1).

9. The Pressurized Ballistics Range is an enclosed steel tube three feet in diameter and 300 feet long (Figure 2). The range can be pressurized to six atmospheres or evacuated down to about 1/100 atmosphere. It is equipped with 25 spark shadowgraph stations, the first 20 stations spaced alternately five and eight feet apart and the last five stations 24.5 feet apart. A bank of 13 counter chronographs is used to measure the time interval between the spark flashes. Descriptions of this range and other ranges at the Naval Ordnance Laboratory are given in reference (a).

10. The one-inch diameter cones were fired from a 30-mm rifled gun (twist one turn in 20.3 calibers) by using a plastic sabot (Figure 3). The resultant Mach numbers are given in Table I. Seven of the models were fired at atmospheric pressure and four of the models at 2/3 of an atmosphere (Table I). Figure 4 shows a typical angle of attack and angle of sideslip motion history for one of the models. The points represent the measured data from the spark shadowgraph stations and the curve is the best "fit" of the linear theory. The results obtained by "fitting" the linear theory to the experimental free-flight data are given in Table II.

11. The values of the aerodynamic coefficients as functions of Mach number are given in Figure 5 where a large spread in the data may be noted. In view of the aerodynamic simplicity of the cone and the dynamic simplicity of the epicyclic fit, it seemed reasonable to attempt to discover the cause of the unexpected large variations in the data from model to model.

12. An examination of the possible sources of error in the epicyclic fit indicated a somewhat poor determination of $\lambda_{1,2}$ resulting from the distribution of the individual round data (Table III). The data were noted to group in two distinct regions, as shown in Figure 4. The determination of the circular center of such a pattern is somewhat inaccurate. However, evaluation of this inaccuracy indicates that it is not sufficient to account for the lack of agreement of the coefficients model to model.

13. Next it seemed reasonable to examine the spark shadowgraphs themselves in the remote hope that perhaps some unusual and systematic flow situation might be revealed. This final effort proved to be fruitful. The nature of the boundary layer was found to be highly varying model to model as well as during the flight of a single model.

14. As a result of this observation, the boundary layer was studied in detail and the results were used in reappraising the experimental aeroballistic coefficient data. This work is reported in the following sections.

Examination of the Boundary Layer

15. The spark shadowgraphs are sensitive to changes in the density gradient and for many years this simple technique has yielded an excellent visualization of the flow field around small missiles in supersonic flight. Besides revealing primary flow features such as the shock waves, the nature of the boundary layer is readily observable (reference (d), (e) and (f).

16. Examination of the spark shadowgraphs obtained during this program revealed very large variations in the boundary-layer transition from model to model and also in most cases during the flight of a single model. Figure 6 shows a complete vertical set of plates for round 2395 obtained as the model flew down the Pressurized Ballistics Range. Large variations in the boundary layer may be observed.

17. In view of the unaccounted for spread in the aerodynamic coefficient data and the large differences in the boundary-layer transition from model to model, it seemed reasonable to attempt a correlation between the two. A simple approach was taken. The percent of the total length of the model which had a laminar boundary layer was measured in each of the vertical shadowgraphs obtained during the flight of a single model.* These measurements were averaged and a probable error was computed. This average and its probable error was used as a criterion for specifying the nature of the varying boundary layer on that particular model.

18. This average may be interpreted as a measure of the average or mean transition point location during the model's flight. Values for this "mean transition" were obtained for each of the models and they are given in Table IV with their probable errors.

19. It may be noted in Table IV that there are large variations in the mean transition between models. A correlation of mean transition with range pressure may, however, be noted. The models with the least laminar flow (i.e., rounds 2390, 2391, 2393, 2394, and 2395) were all tested at atmospheric pressure. All the models with the most laminar flows (i.e., rounds 2389, 2392, 2399, 2401, 2407, and 2408) were tested at reduced range pressure (2/3 atm.) except rounds 2389 and 2392. The change in Reynolds number due to the pressure difference, is believed to be significant in the division of the rounds into the two groups.**

---

* In the case of what we shall call "regular transition" the distances from the nose to the transition points on the upper profile and on the lower profile were averaged to yield a single value of transition distance from each spark shadowgraph (see Figure 7). In the case of what we shall call "chaotic transition" the total laminar distances on the upper profile and on the lower profile were averaged (see Figure 7).

** For purposes of later discussion, the rounds with the most rearward transition are designated the laminar group and those with the most forward transition, the turbulent group.

However, this change would not account for rounds 2389 and 2392 being in the laminar group. It should be recorded that no attempt was made to control or measure the surface finish of any of the models and this may have been a significant parameter for these two rounds.

20. The values for the probable errors of the mean transition are indicative of the fluctuation in the transition point which occurs during the model's flight down the range. The truly transient nature of the location of the transition point is specified by computing this quantity. It is suggested that future determinations of the transition point might be made useful and physically representative if its probable error was also computed.

21. These values of mean transition provided the necessary specification of the nature of the boundary layer existing on each of the models during its flight, and, thus, suggest the possibility of correlating the variable boundary-layer conditions with the dispersion in the aeroballistic coefficient data. This correlation is considered in the following section.

Data Correlation

22. The aerodynamic coefficient data for the normal force, restoring moment, damping and lag moments, and Magnus moment (i.e., C_{N_α}, C_{M_α}, $C_{M_q} + C_{M_{\dot{\alpha}}}$, $C_{M_{p\alpha}}$) are plotted versus mean transition in Figures 8 through 11.

23. Weighted linear fits were made to all the coefficient data and are illustrated by the solid lines in the plots.* The weights were based on the probable errors of the individual coefficients and equaled $1/PE^2$. In addition, the data were also considered as divided into two seperate groups, a laminar group and a turbulent group, as indicated previously. The dotted lines on the plots represent these averages.

24. Table V gives the weighted averages and their probable errors, and the weighted linear equations and their probable errors.

25. It appears from this correlation that both the static and dynamic aerodynamic coefficients for a pure cone in supersonic flight are significantly dependent on the nature of boundary layer.

---

* Unweighted linear fits were also made and included for completeness.

Discussion of Results

26. The normal force, damping and lag moment, and Magnus moment all show improved determinations, based on their probable errors, when considered as varying with mean transition. The restoring moment shows no significant change; but, because of the small static margin for the models tested, this coefficient is so poorly determined that no consideration should be given to it. Table VI lists the average coefficient data as originally computed, the weighted averages for the data grouped in laminar and turbulent groups, and the laminar and turbulent values computed from the weighted linear fits.*

27. Since the Magnus moment, which was of primary interest, still showed a large dispersion, additional attempts were made to improve its determination. It was noted that the yawing motions of the rounds (Figure 4) were such that the damping factors for the nutation and precession arms were difficult to determine. Table III lists the damping factors and their probable errors. An attempt was thus made to compute the Magnus moment coefficient by a modified data reduction procedure which uses the damping factors for the nutation and precession arms separately. Two sets of these modified coefficients were computed; one based on weighted average values of C_{N_α} and $C_{M_q} + C_{M_{\dot{\alpha}}}$, the other based on the weighted least square lines fitted to the data. The results of these are given in Figures 12 and 13.

28. As may be noted in the figures, no obvious improvement in the data was obtained by this alternative approach. It was reported here only for completeness and perhaps to aid future investigators.

29. Finally, it is believed that the remaining spread in the Magnus moment coefficient data may be due to three primary factors: (1) the poorly determined values for the mean transition**, (2) the distribution and nature of the range data on this program, and (3) perhaps the most important, on the chaotic nature of the boundary layer on many of the rounds.

---

* Since there was a Mach number variation which was not considered when treating the data as a whole, a similar table based on 8 rounds whose Mach number variation was less than 0.1 was also computed (Table VII). Slightly improved results were obtained.

**. It should be recalled that only the profile boundary layer was observed in the vertical spark shadowgraph. The state of the boundary layer over the rest of the model's surface was completely unknown and thus not represented by the values for the mean transition.

30. In the following section the experimental values for the aerodynamic coefficients on a cone will be compared with various theoretical predictions.

Comparison with Theory

Normal Force and Restoring Moment

31. Exact theory for the normal force and its moment on a pure cone in supersonic flow is given by Stone (reference (g)) and computed by Kopal (reference (h)). Approximate values may be obtained from Munk's (reference (i) and (j)) airship theory. Values may also be computed by Newtonian theory (reference (k)). These theoretical values are given in Table VIII together with values computed from the weighted linear fits for the cases of fully laminar and fully turbulent boundary layer. It is noted that the three theoretical values for the normal force fall within the range of the values for fully laminar and fully turbulent boundary layer obtained by extrapolation from the experimental values. The experimental values for the restoring moment are not in good agreement with the theoretical predictions; however, the coefficients are small and within the accuracy of measurements and thus, as indicated earlier, subject to large errors.

Damping and Lag Moment

32. Estimates for the damping moment may also be obtained from Munk's airship theory, strip theory using Kopal, and from Newtonian theory. Values for these three estimates are also given in Table VIII together with values extrapolated from the experimental data.

Magnus Moment

33. During the conduct of the program, two methods for predicting the Magnus force and moment on cones in supersonic flow became available. One method reported by both Sedney (reference (l)) and Fiebig (reference (m)) is based on distortion of the boundary layer due to spin, and the other, reported by Parrish (reference (k)), is based on a Newtonian type concept.*

---

* The Newtonian values for Magnus force and moment may also be obtained if a Maxwellian-Diffuse model of molecular reflection is used (reference (n) and (o)).

34. The predictions by these two methods are given in Table VIII and plotted in Figure 14 together with the experimental data. The theoretical value of Sedney and Fiebig, although only applicable to the laminar case, is nevertheless considerably less than the extrapolated completely laminar experimental value.

35. The theoretical value obtained by the Newtonian method is in poor agreement with the extrapolated experimental value for the completely turbulent boundary layer, but is in considerably better agreement with the completely laminar value.

36. Clearly neither method of prediction is in good agreement with the experimental data. Since the accuracy of the experimental data has been shown to be considerably better than the differences between theory and experiment, some lack of confidence in the theoretical predictions may be justified.

37. Experimental values for the Magnus force would be most helpful in correlating with theory and possibly as a guide for the development of theory. Future programs should determine this force.

CONCLUSION

38. The experimental values for the static and dynamic aerodynamic coefficients (C_{N_α}, C_{M_α}, $C_{M_q} + C_{M_{\dot\alpha}}$, and $C_{M_{p\alpha}}$) for a pure spinning cone in supersonic flight were determined from model firings in the NOL Pressurized Ballistics Range.

39. Regular and chaotic boundary-layer transition was observed during the flight of the models from the spark shadowgraph data and was found to be represented by a mean transition distance and its probable error.

40. The experimental aerodynamic coefficient data (C_{N_α}, $C_{M_q} + C_{M_{\dot\alpha}}$, and $C_{M_{p\alpha}}$) were found to be significantly dependent on the nature of the boundary layer (mean transition).

41. Various methods for the theoretical prediction of C_{N_α} and $C_{M_q} + C_{M_{\dot\alpha}}$ yield values within the variations of the experimental data due to boundary-layer transition. The theoretical predictions for the Magnus moment $C_{M_{p\alpha}}$ were poor.

42. Further experimental investigations of Magnus effects in aeroballistic ranges and wind tunnels appear to be required, and are, therefore, recommended. Care should be taken in future programs

(a) to avoid chaotic transition by control of the nature of the boundary layer (i.e., surface finish, boundary-layer trips, range pressure, etc.),

(b) to use range models with forward c.g.'s,

(c) to extend the studies to large values of the angle of attack and a larger range of Mach number, particularly hypersonic and transonic, and

(d) to measure the Magnus force.

References

(a) May, A. and Williams, T. J., Free-Flight Ranges at the Naval Ordnance Laboratory, NavOrd Report 4063 (1955)

(b) Murphy, C. H., Data Reduction for the Free Flight Spark Ranges, BRL Report No. 900 (1954)

(c) Nicolaides, J. D., Firing Range Method of Obtaining Aerodynamic Data Appendix C, Dragonfly Summary Report (MX-802), General Electric Company (1948)

(d) Witt, Jr., W. R., Free-Flight Determination of the Boundary-Layer Transition of Cone Cylinders, Paper presented at Annual Meeting of The American Physical Society, New York, New York (1952)

(e) Gazley, Carl, Boundary Layer Stability and Transition on Subsonic and Supersonic Flow, Journal of the Aeronautical Sciences, Vol. 20, No. 1 (1953)

(f) Nicolaides, J. D. and Karpox, B. G., On the Free Flight Drag Determination of a Finned Configuration Flying at Critical Reynolds Number, BRL Report No. 751 (1953)

(g) Stone, The Aerodynamics of a Slightly Yawing Supersonic Cone, NDRC Report Div. 1 (1944)

(h) Kopal, Z., Tables of Supersonic Flow Around Yawing Cones, MIT Report (1947)

(i) Munk, M., Aerodynamic Theory of Airships, Volume VI, Aerodynamic Theory (1934)

(j) Wood, R. M. and Murphy, C. H., Aerodynamic Derivatives for Both Steady and Non-Steady Motion of Slender Bodies, BRL No. 880 (1955)

(k) Parrish, G. B., Comparison of Aerodynamic Coefficients for a Cone as Computed from Some Simple Available Procedures, BuOrd TN No. 38 (1957)

(l) Sedney, R., Laminar Boundary Layer on a Spinning Cone at Small Angles of Attack, BRL Report No. 991 (1956)

(m) Fiebig, M., Laminar Boundary Layer on a Spinning Circular Cone in Supersonic Flow at a Small Angle of Attack, Cornell University Report, Volx. I and II, (June 1956 and February 1957)

(n) Kuhlthau, A. R., Application of High Rotational Speed Techniques to the Measurement of Viscous Drag in Gases, University of Virginia Rpt (1955)

References (Cont'd)

(o) Finch, T. W., Stability Derivatives for Spinning Bodies of Revolution in the Superaerodynamic Region, BuOrd TN No. 43 (1958)

List of Symbols

C_D	drag coefficient = D/qS
C_{ℓ_p}	slope of roll damping coefficient = $L_p p / \frac{pd}{2V} QSd$
C_{M_α}	slope of pitching moment coefficient = $M_\alpha \alpha / QSd\alpha$
$C_{M_{p\alpha}}$	slope of Magnus moment coefficient = $M_{p\alpha} p\alpha / \frac{pd}{2V} QSd\alpha$
$C_{M_q} + C_{M_{\dot\alpha}}$	slope of yaw damping moment = $M_q q / \frac{d}{2V} QSd + M_{\dot\alpha} \dot\alpha / \frac{\dot\alpha d}{2V} QSd$
C_{N_α}	slope of normal force coefficient = $N_\alpha \alpha / QS\alpha$
C.G.	center of gravity
d	maximum body diameter
I	transverse moment of inertia
I_X	axial moment of inertia
$K_{1,2}$	magnitude of "nutation" and "precession" arms
L	model length
ℓ_T	mean transition distance
M	Mach number
M.T.	mean transition - % of total length
m	mass in grams
p	spin rate
P.E.	probable error
Q	dynamic pressure = $1/2(\rho V^2)$
q	pitching velocity

List of Symbols (Cont'd)

Re	Reynolds number = $\frac{\rho VL}{\mu}$
S	maximum cross-sectional area = $\frac{\pi d^2}{4}$
s	stability factor
V	down range velocity
$\tilde{\alpha}$	complex angle of attack
δ^2	mean squared yaw
$\lambda_{1,2}$	damping factors associated with the "nutation" and "precession" arms
μ	coefficient of viscosity
ρ	density of air
τ	$= \frac{1}{\sqrt{1 - \frac{1}{s}}}$
$\omega_{1,2}$	rotation rates of the "nutation" and "precession" arms

TABLE I

Mach Numbers and Range Pressures
for Each Shot

Round Number	Mach Number	Range Pressure (inches of Hg)
2389	2.07	29.7
2390	2.31	29.7
2391	2.29	29.9
2392	2.32	29.8
2393	2.24	29.3
2394	2.27	30.1
2395	2.35	30.1
2399	2.30	19.8
2401	2.02	19.6
2407	1.75	19.9
2408	2.28	19.7

TABLE II

Tabulation of Results

Round Symbol	2390 ○	2391 △	2393 □	2394 ▽	2395 ◇
C_D	0.273	0.276	0.283	0.278	0.271
P.E. in C_D	±0.001	±0.001	±0.002	±0.001	±0.002
M	2.31	2.29	2.24	2.27	2.35
Re x 10^{-6}	3.67	3.68	3.57	3.17	3.76
δ^2 - deg^2	0.57	0.84	3.58	1.56	0.98
τ	0.9960	0.9911	0.9940	0.9921	0.9980
C_{M_α}	-0.018	-0.049	-0.030	-0.041	-0.008
P.E.	±0.008	±0.006	±0.006	±0.007	±0.007
C_{N_α}	-1.821	-1.930	-1.656	-1.350	-1.658
P.E.	±0.353	±0.276	±0.280	±0.196	±0.327
$C_{M_q} + C_{M_{\dot\alpha}}$	-2.804	-2.348	-3.114	-3.304	-2.843
P.E.	±0.516	±0.408	±0.377	±0.367	±0.418
$C_{M_{p\alpha}}$	0.248	0.112	0.192	0.278	0.268
P.E.	±0.085	±0.066	±0.028	±0.057	±0.073
P.E. in Yaw (radians)	0.0011	0.0009	0.0016	0.0012	0.0009
P.E. in Swerve (inches)	0.012	0.017	0.024	0.014	0.013
CG from Base (calibers)	0.911	0.910	0.909	0.909	0.908

NOTE: An average C_p (-0.007) was used for all rounds

TABLE II (Cont'd)

Round	2389	2392	2399	2401	2407
Symbol					
C_D	0.302	0.273	0.289	0.309	0.356
P.E. in C_D	±0.001	±0.001	±0.001	±0.001	±0.002
M	2.07	2.32	2.30	2.02	1.75
Re x 10^{-6}	3.30	3.72	2.42	2.12	1.88
δ^2 - deg^2	1.09	0.80	6.34	1.24	3.21
τ	0.9940	0.9980	0.9940	0.9940	1.010
C_{M_α}	-0.030	-0.013	-0.043	-0.043	0.074
P.E.	±0.011	±0.012	±0.006	±0.013	±0.020
C_{N_α}	-2.430	-2.250	-2.048	-1.958	-2.318
P.E.	±1.424	±0.994	±0.391	±0.863	±0.946
$C_{M_q} + C_{M_{\dot\alpha}}$	-0.413	-2.934	-1.851	-1.916	-1.263
P.E.	+1.234	+0.965	+0.390	+0.954	+1.279
$C_{M_{p\alpha}}$	-0.312	-0.024	-0.091	-0.119	-0.137
P.E.	±0.205	±0.153	±0.065	±0.147	±0.204
P.E. in Yaw (radians)	0.0012	0.0012	0.0012	0.0014	0.0024
P.E. in Swerve	0.014	0.013	0.012	0.011	0.010
CG from Base (calibers)	0.910	0.910	0.914	0.911	0.876

TABLE II (Cont'd)

Round	2408
Symbol	▷
C_D	0.283
P.E. in C_D	±0.002
M	2.28
Re x 10^{-6}	2.40
δ^2 Deg^2	1.03
τ	0.9960
C_{M_α}	-0.025
P.E.	±0.016
C_{N_α}	-1.931
P.E.	±1.077
$C_{M_q} + C_{M_{\dot{\alpha}}}$	-2.362
P.E.	±1.306
$C_{M_{p\alpha}}$	-0.013
	±0.206
P.E. in Yaw (radians)	0.0017
P.E. in Swerve (inches)	0.011
CG from Base (calibers)	0.880

TABLE III

Damping Factors

Round No.	$\lambda_1 \times 10^3$	P.E.	P.E.(%)	$\lambda_2 \times 10^3$	P.E.	P.E. (%)
2389	-3.679	±0.825	22.4	-0.746	+0.756	101.3
2390	-3.696	±0.750	20.3	-4.928	±0.576	11.7
2391	-3.707	±0.541	14.6	-3.806	±0.418	11.0
2392	-6.289	±0.774	12.3	-3.123	±0.795	25.4
2393	-4.859	±0.461	9.5	-4.120	±0.470	11.4
2493	-4.068	±0.480	11.8	-4.412	±0.464	10.5
2395	-3.854	±0.501	12.9	-4.755	±0.547	11.5
2399	-3.172	+0.209	6.6	-1.425	+0.280	19.6
2401	-3.345	±0.622	18.6	-1.151	±0.597	51.9
2407	-2.672	±0.976	36.5	-1.696	±0.971	57.2
2408	-3.425	±0.935	27.3	-2.104	±0.774	36.8

TABLE IV

Mean Transition

Round	Range Pressure (inches of Hg)	Mean Transition (% of length)	P.E. in Mean Transition (% of Length)
2390	29.7	33.5	12.6
2391	29.9	43.8	15.2
2393	29.8	36.7	8.7
2394	30.1	30.0	5.9
2395	30.1	55.7	18.0
2389	29.7	86.7	12.0
2392	29.8	84.3	21.5
2399	19.8	90.6	7.5
2401	19.6	68.3	11.1
2407	19.9	100.0	0.0
2408	19.7	85.5	10.9

TABLE V

Weighted Average Coefficients

1. Weighted Average Coefficients for the Laminar and Turbulent Groups

	Mean Transition	
Coefficient	86%	40%
C_{N_α}	-2.09	-1.61
P.E.	±0.13	±0.14
P.E. (%)	6.4	8.7
C_{M_α}	-0.031	-0.031
P.E.	±0.030	±0.010
P.E. (%)	96.8	32.2
$C_{M_q} + C_{M_{\dot{\alpha}}}$	-1.87	-2.92
P.E.	±0.54	±0.22
P.E. (%)	28.9	7.5
$C_{M_{p\alpha}}$	-0.098	0.204
P.E.	±0.068	±0.042
P.E. (%)	69.4	20.6

2. Weighted Linear Equations for Coefficients as Functions of Mean Transition Distance (ℓ_T)

$C_{N_\alpha} = -1.05 - 0.475\ell_T$
P.E. of Fit = ±0.14

$C_{M_\alpha} = -0.031 - 0.002\ell_T$
P.E. of Fit = ±0.027

$C_{M_q} + C_{M_{\dot{\alpha}}} = -3.80 + 0.76\ell_T$
P.E. of Fit = ±0.46

$C_{M_{p\alpha}} = 0.379 - 0.177\ell_T$
P.E. of Fit = ±0.080

TABLE VI

Comparison of Average Coefficient Data
Computed by Various Techniques
(based on all 11 rounds)

	Average for Ungrouped Data	Weighted Averages		Computed from Weighted Linear Equations	
		Laminar Group (M.T. 86%)	Turbulent Group (M.T. 40%)	Laminar Group (M.T. 86%)	Turbulent Group (M.T. 40%)
C_{N_α}	-1.94	-2.09	-1.61	-2.21	-1.59
P.E.	±0.20	±0.13	±0.14	±0.14	
C_{M_α}	-0.02	-0.03	-0.03	-0.04	-0.03
P.E.	±0.03	±0.03	±0.01	±0.03	
$C_{M_q} + C_{M_{\dot{\alpha}}}$	-2.29	-1.87	-2.92	-1.94	-2.93
P.E.	±0.56	±0.54	±0.22	±0.46	
$C_{M_{p\alpha}}$	+0.04	-0.10	0.20	-0.05	0.18
P.E.	±0.13	±0.07	±0.04	±0.08	

TABLE VII

Comparison of Average Coefficient Data
Computed by Various Techniques
(based on 8 rounds where Mach number variation was less than ±0.1)

	Average for Ungrouped Data	Weighted Averages		Computed from Weighted Linear Equations	
		Laminar Group (M.T. 86)	Turbulent Group (M.T. 40%)	Laminar Group (M.T. 86%)	Turbulent Group (M.T. 40%)
C_{N_α}	-1.83	-2.06	-1.61	-2.21	-1.59
P.E.	±0.17	±0.13	±0.14	±0.17	
C_{M_α}	-0.03	-0.04	-0.03	-0.04	-0.03
P.E.	±0.01	±0.02	±0.01	±0.01	
$C_{M_q} + C_{M_{\dot\alpha}}$	-2.70	-2.03	-2.92	-1.96	-2.94
P.E.	±0.299	±0.57	±0.22	±0.33	
$C_{M_{p\alpha}}$	0.12	-0.08	0.20	-0.05	+0.18
P.E.	±0.09	±0.05	±0.04	±0.05	

TABLE VIII

Comparison of Measured and Theoretical Values for Some Aerodynamic Coefficients

	Computed from Measured Data	Computed Values Based on Various Theories: Kopal*	Strip with Kopal*	Munk	Newtonian	Fiebig, Sedney
C_{N_α}	-2.38L -1.05T	-1.86	--	-2.00	-1.94	--
C_{M_α}	-0.037L -0.031T	-0.041	--	+0.072	-0.043	--
$C_{M_q} + C_{M_{\dot{\alpha}}}$	-1.62L -3.70T	--	-1.73	-2.54	-1.85	--
$C_{M_{p\alpha}}$	-0.13L +0.38T	--	--	--	-0.38	-0.005

* evaluated at Mach 5.0

L completely laminar M.T. 100%

T completely turbulent M.T. 0%

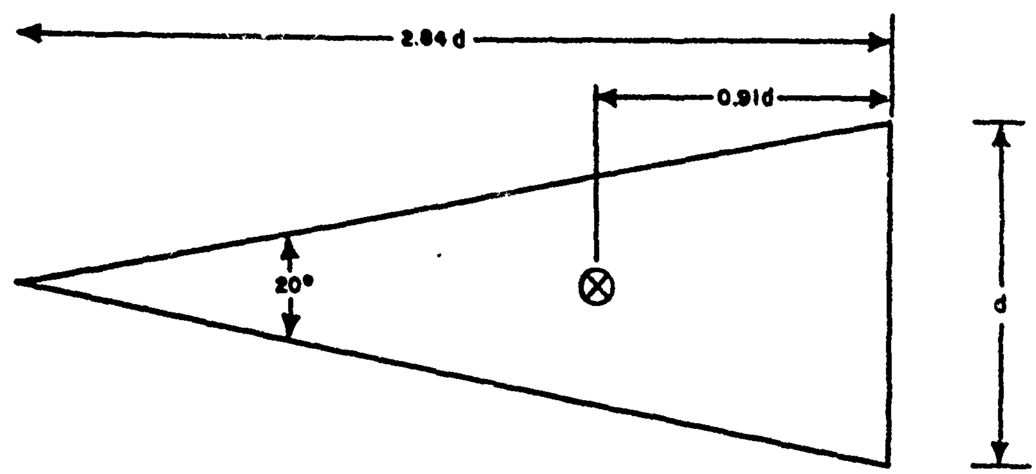

FIG. 1

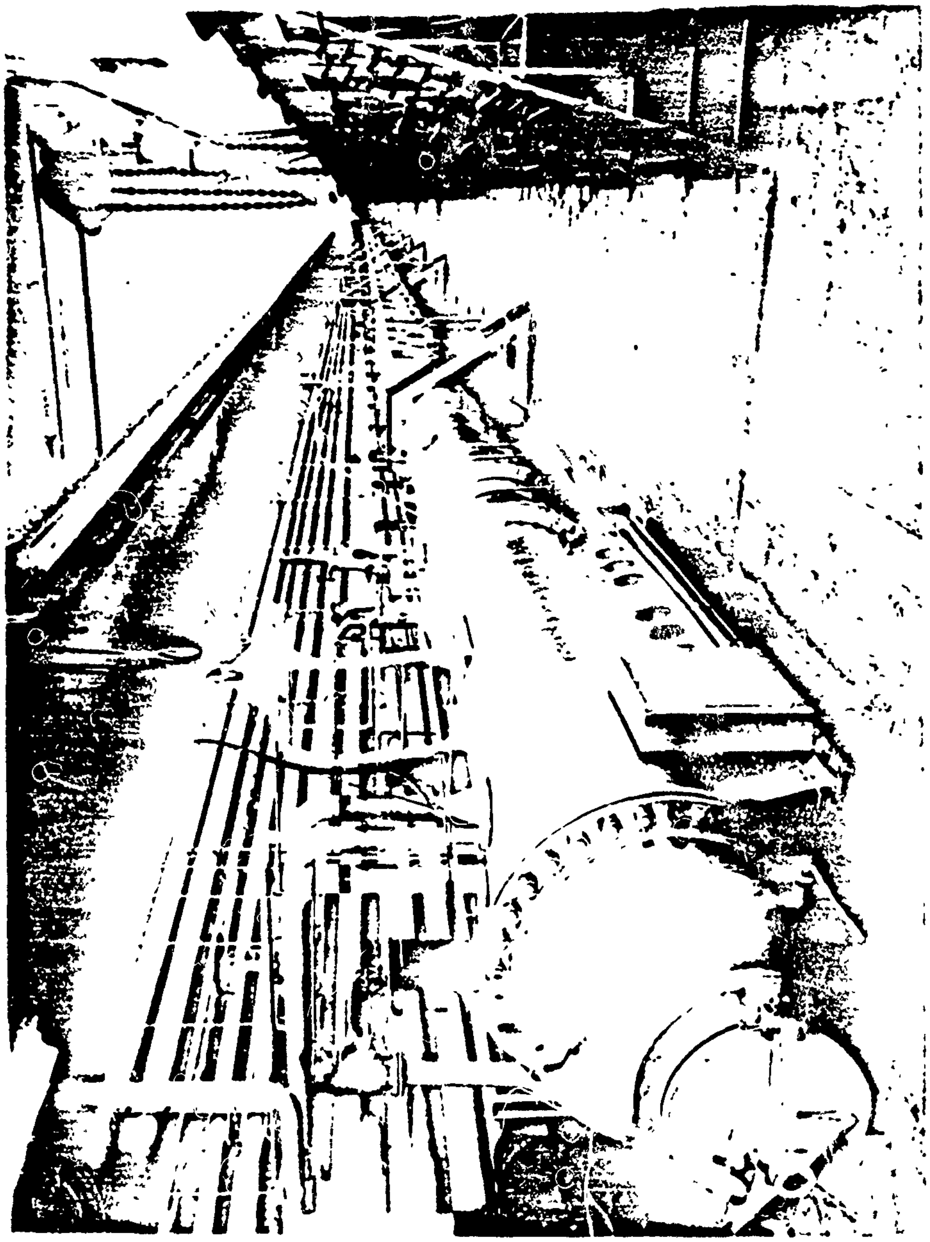

FIG. 2 PRESSURIZED BALLISTICS RANGE

FIG. 3 SPIN CONE MODEL AND LAUCHING SABOT

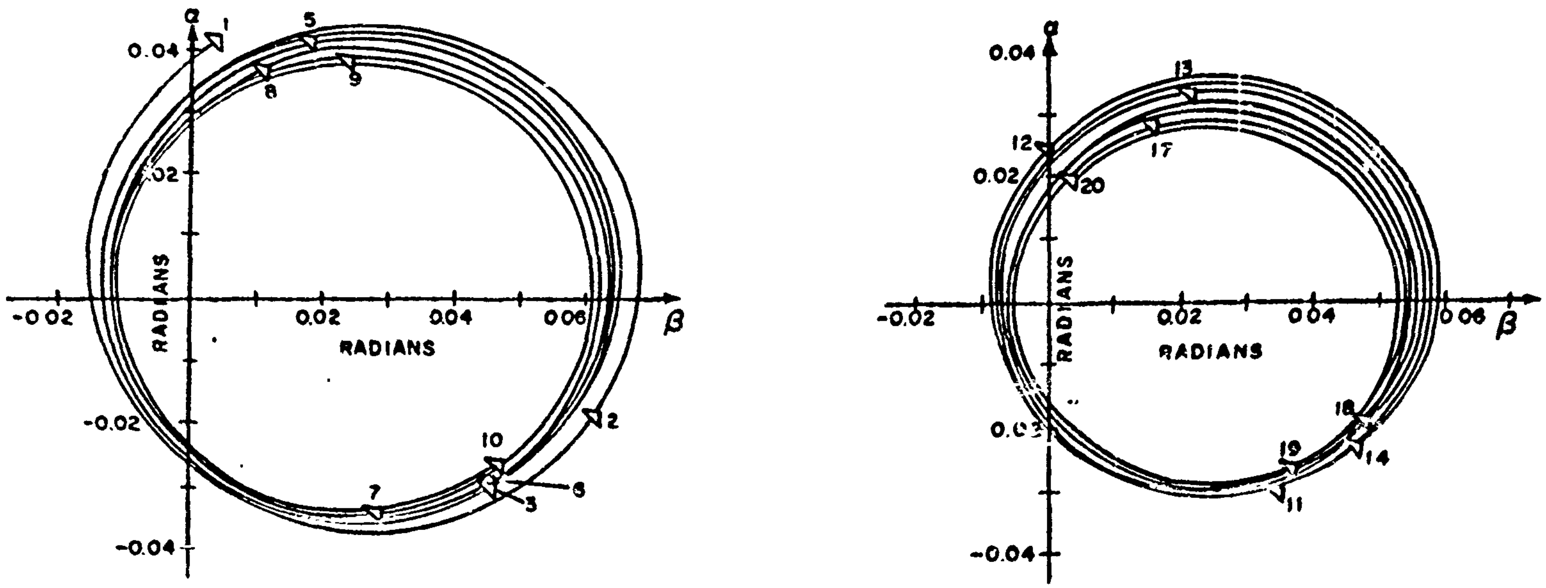

STATIONS 1-10 ∿6.5 NUTATIONS

STATIONS 11-20 ∿6.3 NUTATIONS

FIG.4 TYPICAL YAWING MOTION (ROUND 2399)

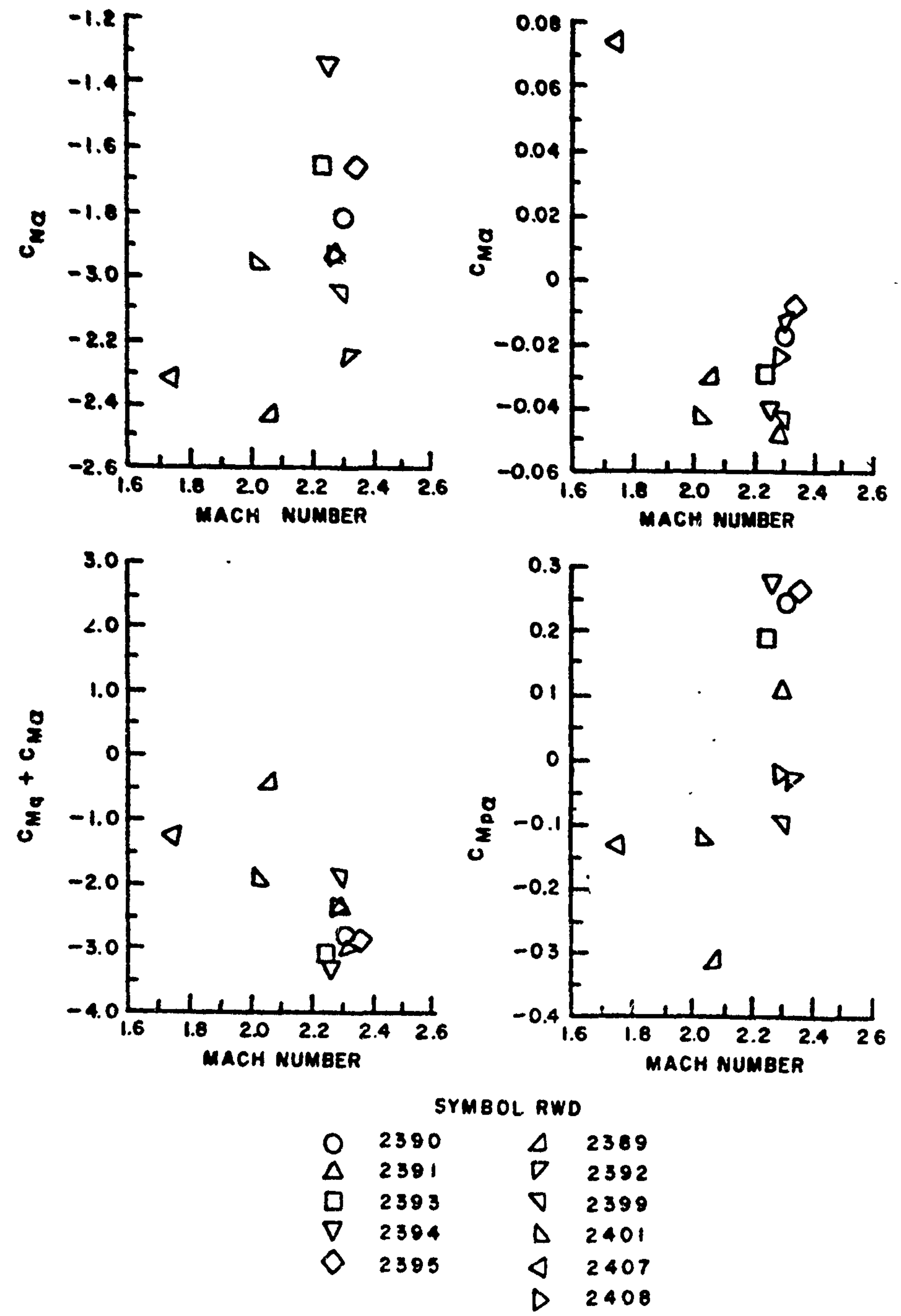

FIG. 5 AERODYNAMIC COEFFICIENTS VS MACH NUMBER

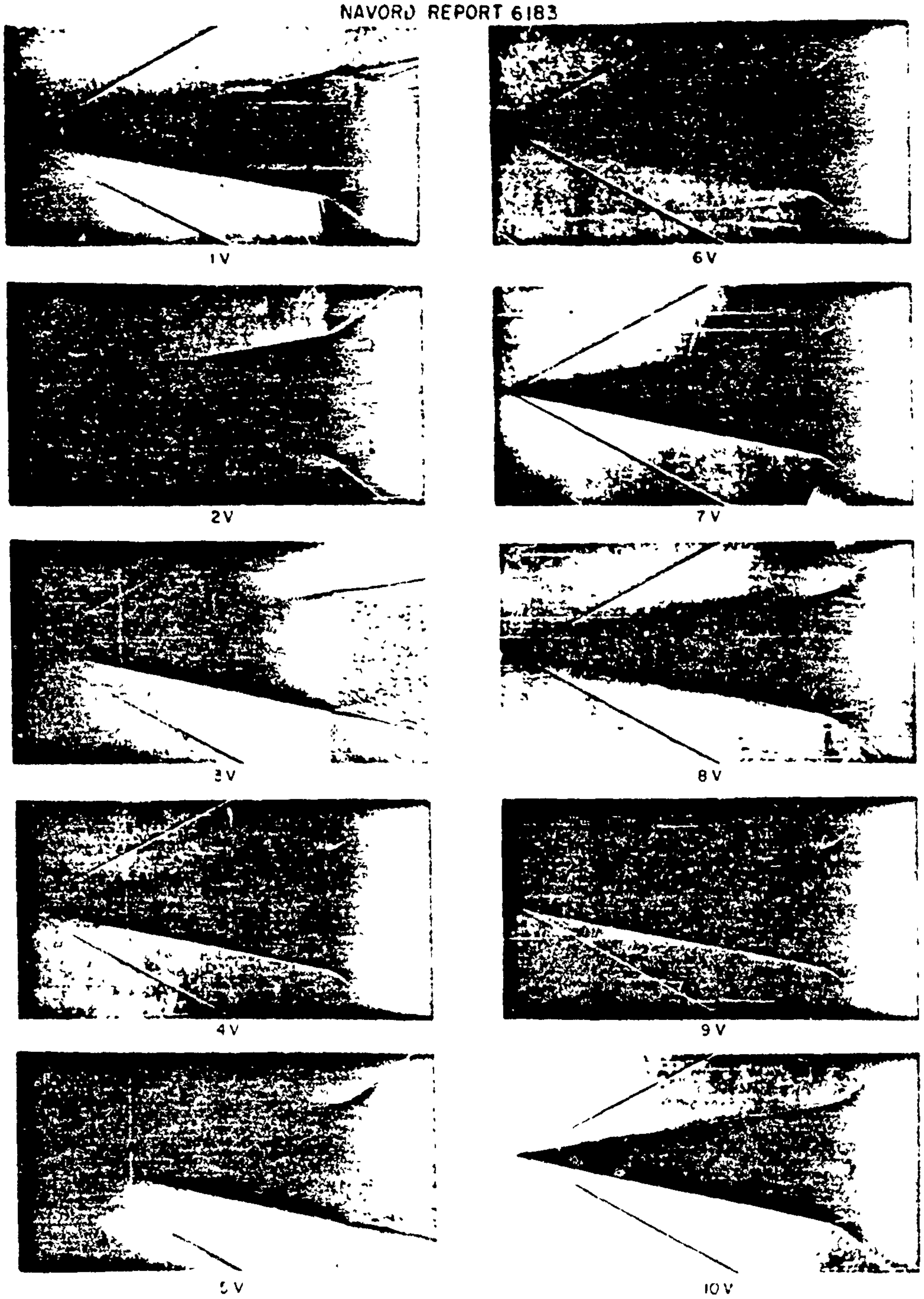

FIG.6A PRINTS OF VERTICAL PLATES FOR ROUND NO.2395
(STATION 1-10)

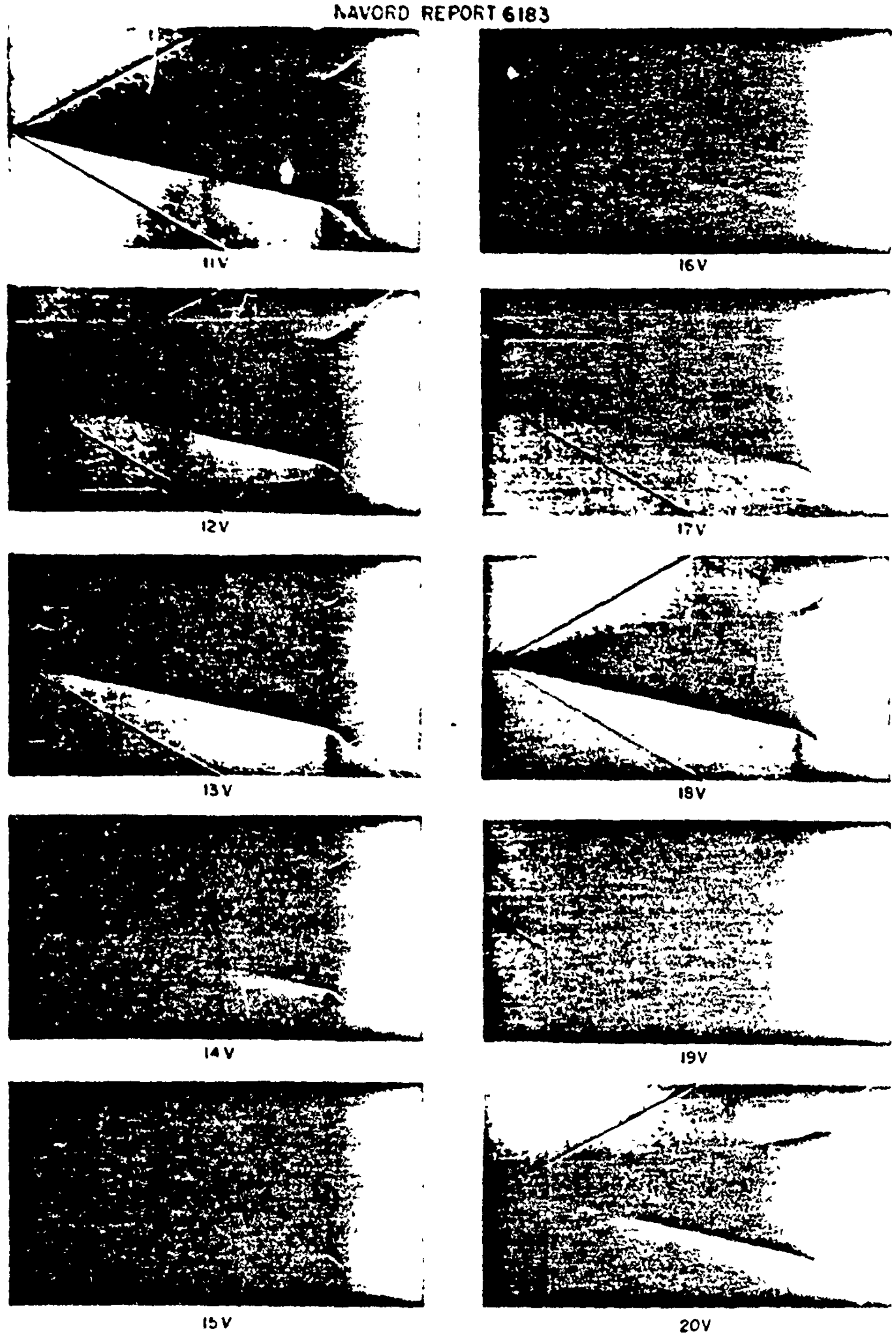

FIG.6B PRINTS OF VERTICAL PLATES FOR ROUND NO.2395
(STATION 11-20)

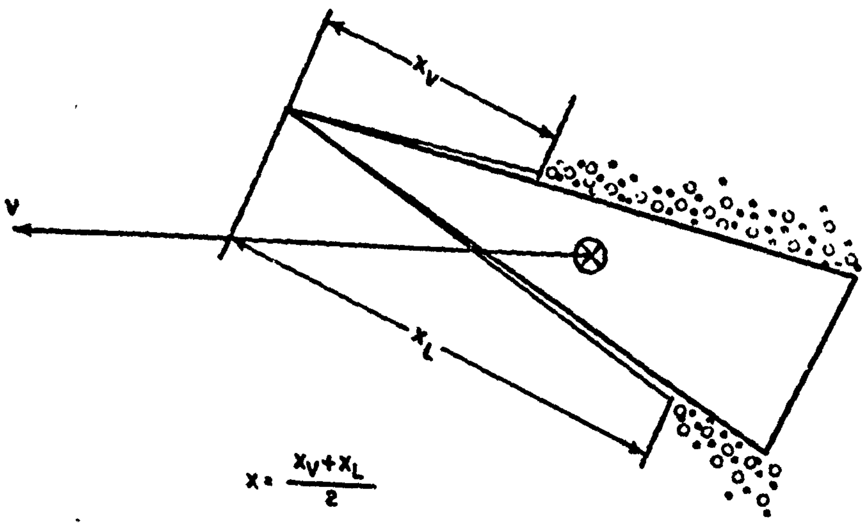

$$X = \frac{X_V + X_L}{2}$$

REGULAR TRANSITION

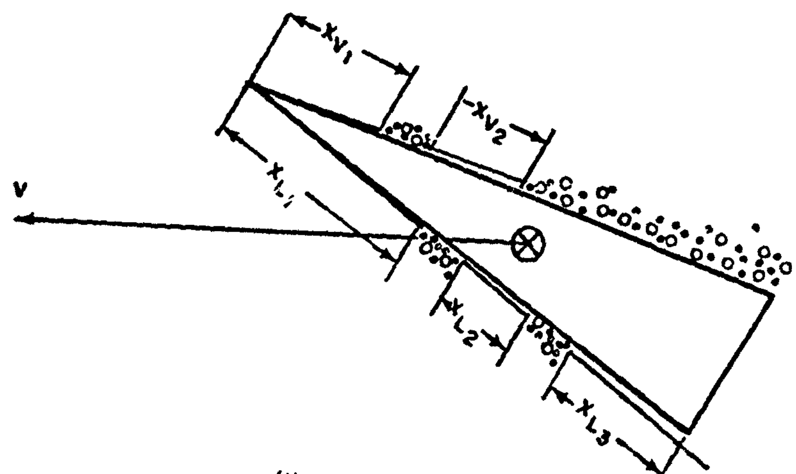

$$X = \frac{(X_{V_1} + X_{V_2}) + (X_{L_1} + X_{L_2} + X_{L_3})}{2}$$

CHAOTIC TRANSITION

FIG. 7 REGULAR AND CHAOTIC TRANSITION

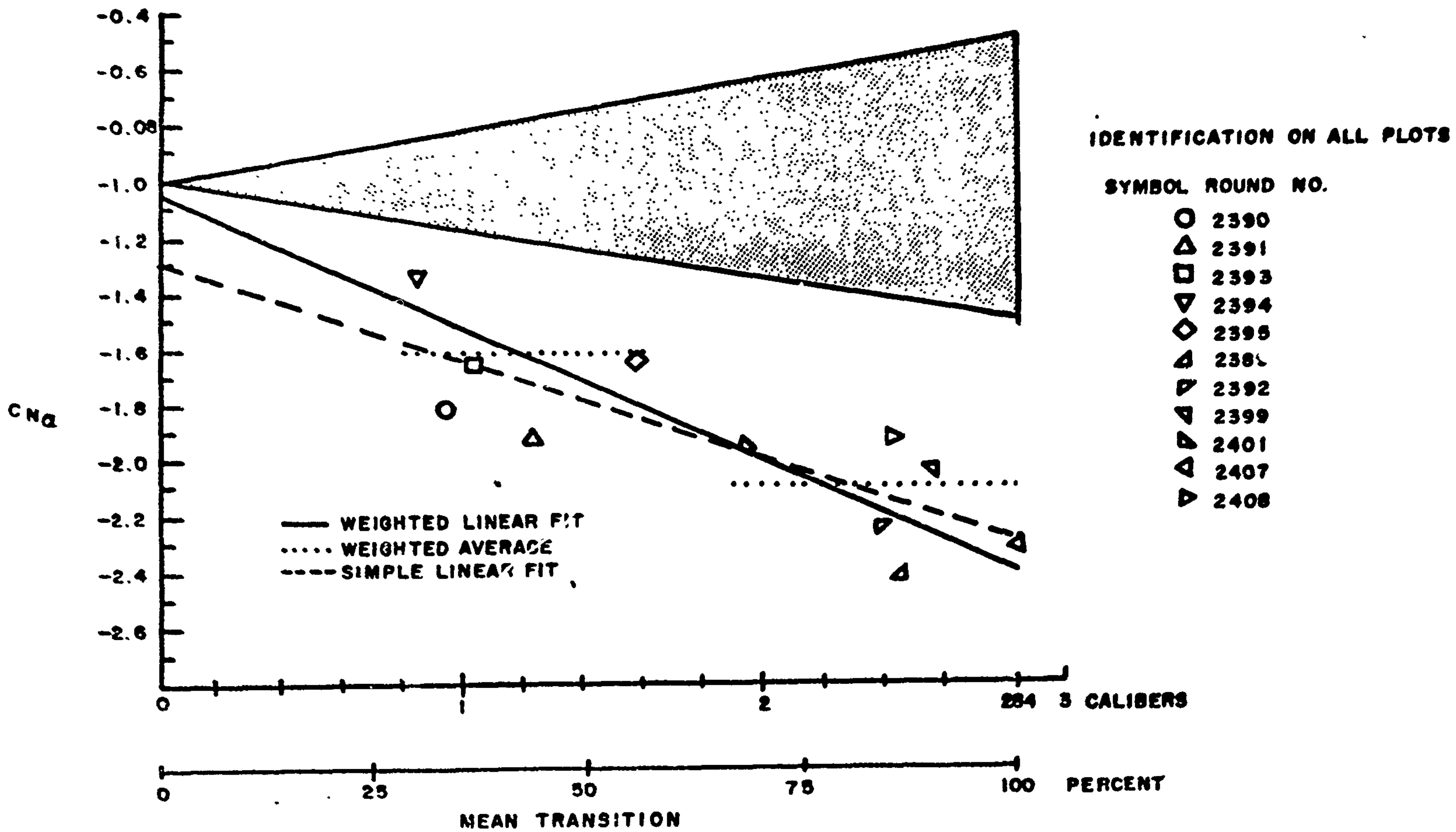

FIG 8 $C_{N\alpha}$ VS MEAN TRANSITION

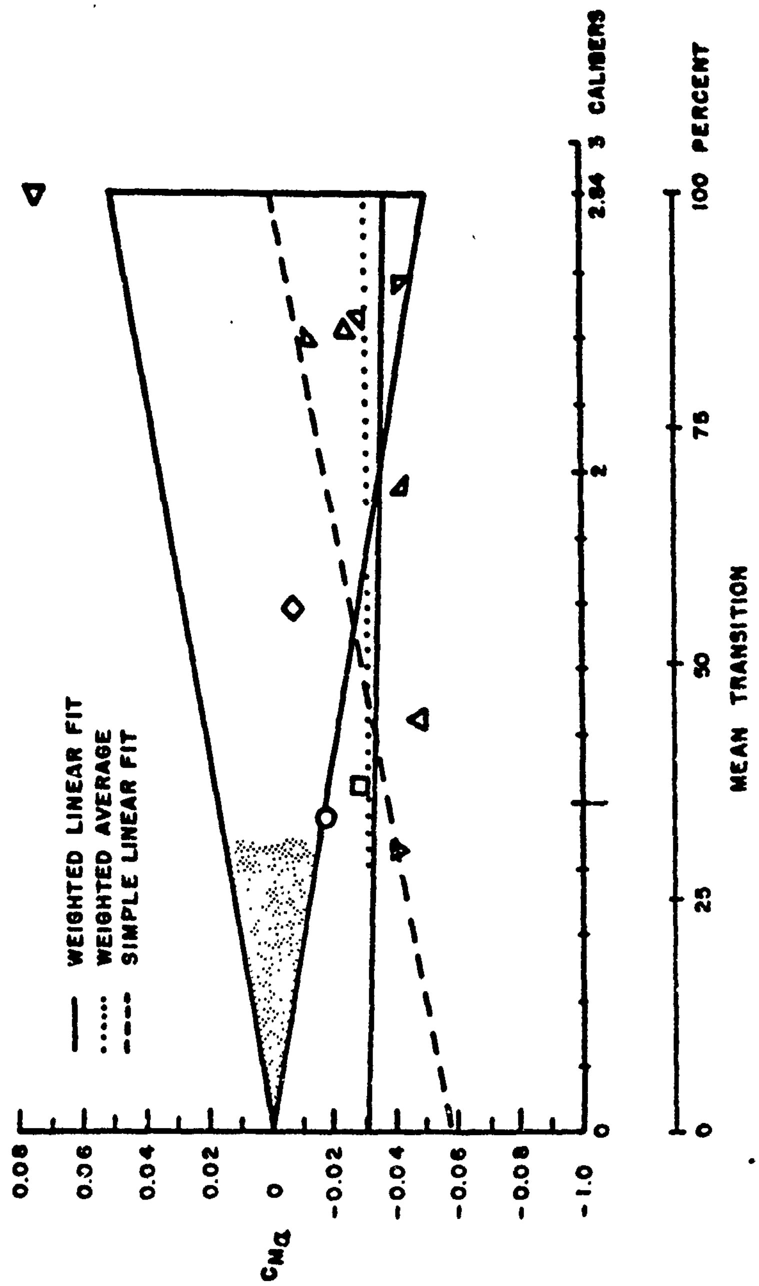

FIG 9 C_{M_α} VS MEAN TRANSITION

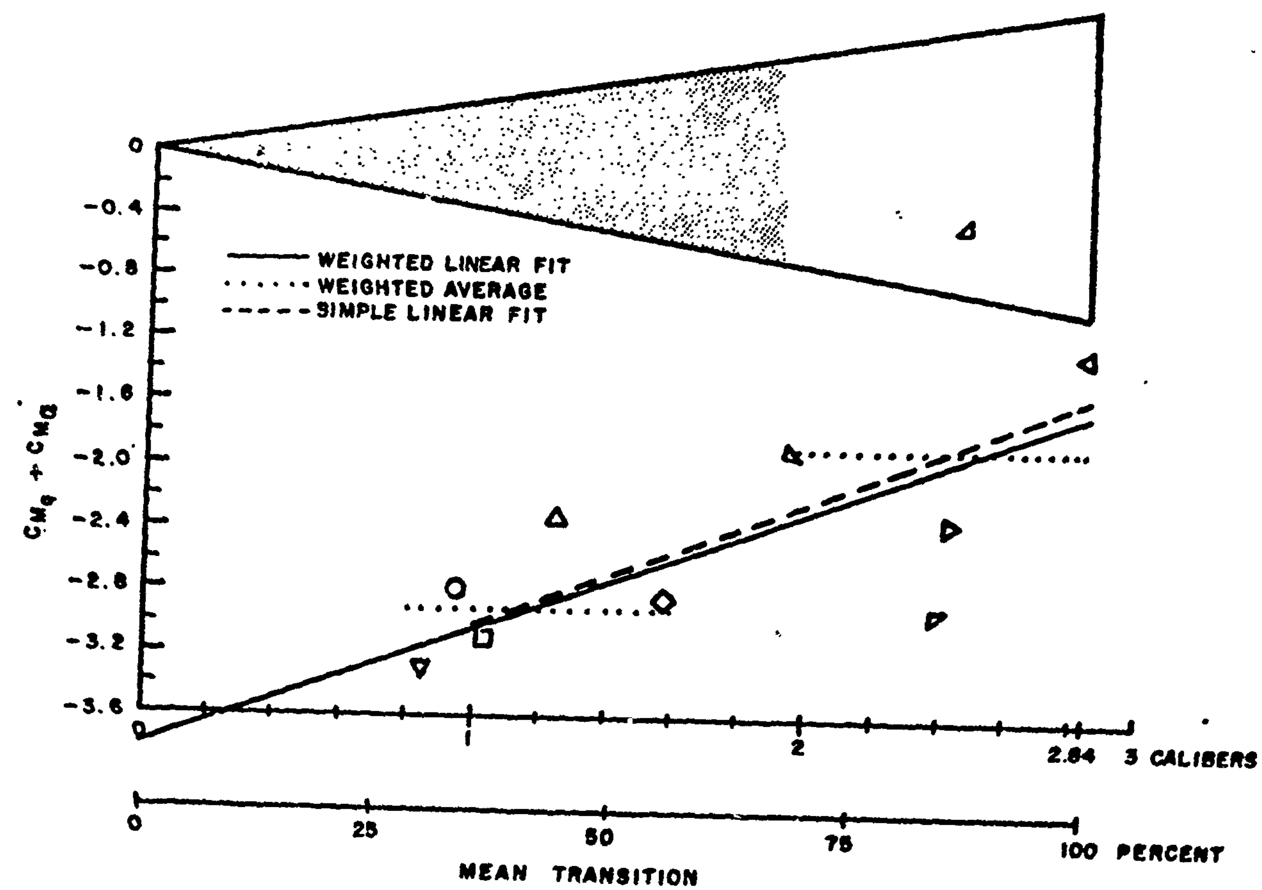

FIG 10 $C_{M_q} + C_{M_\alpha}$ VS MEAN TRANSITION

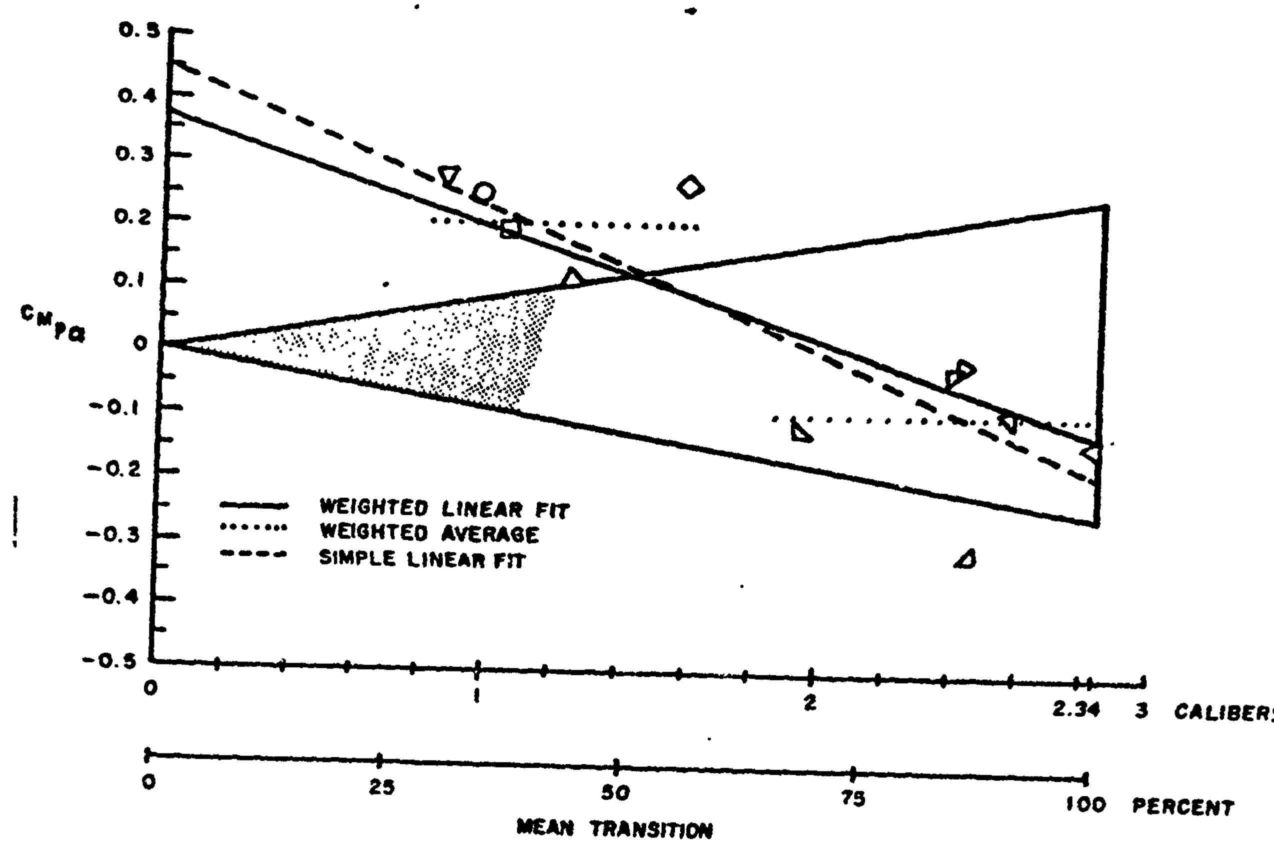

FIG 11 $C_{M_{p\alpha}}$ VS MEAN TRANSITION

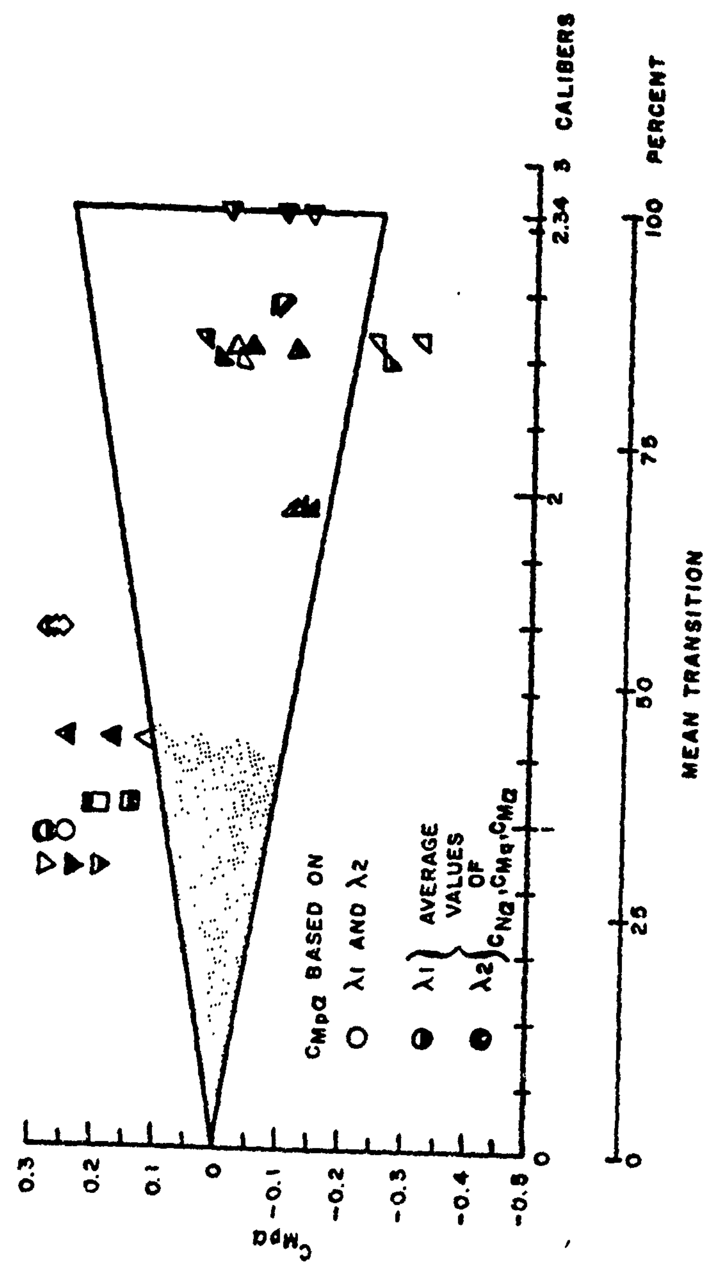

FIG. 12 $C_{Mp\alpha}$ VS MEAN TRANSITION

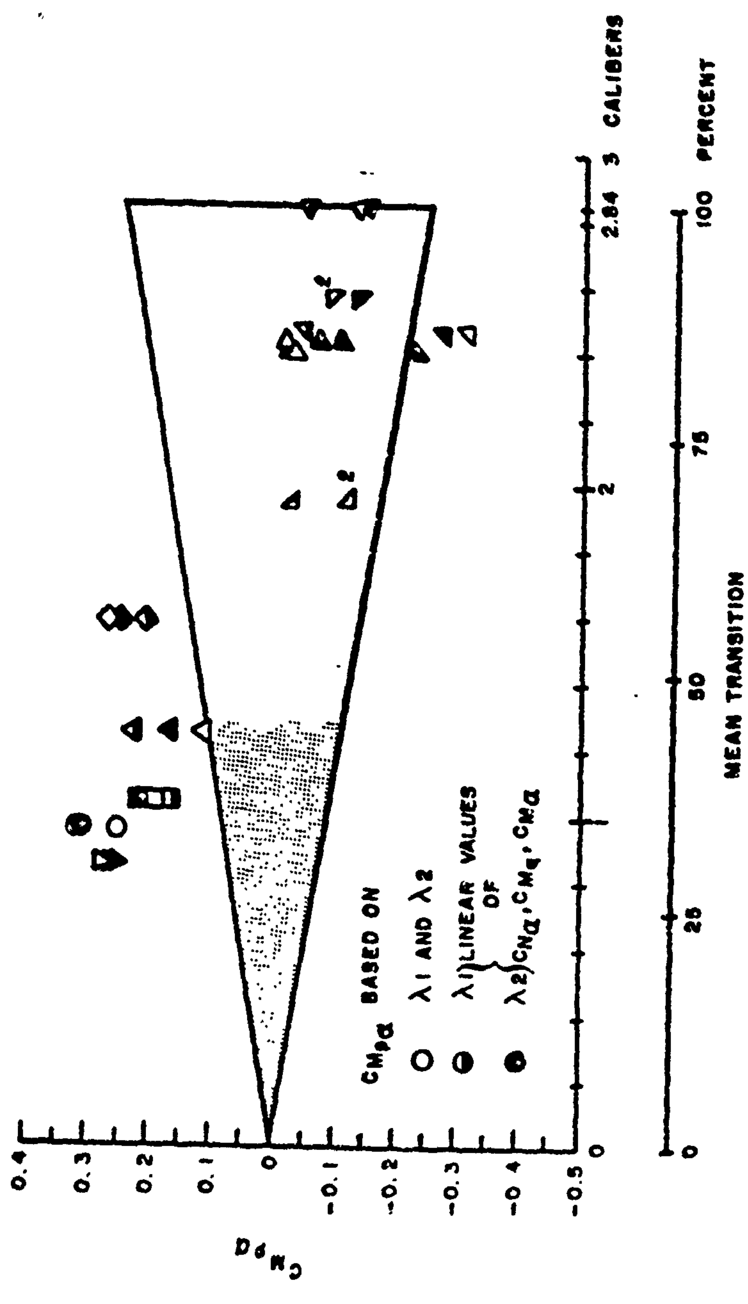

FIG 13 $C_{M_{p\alpha}}$ VS MEAN TRANSITION

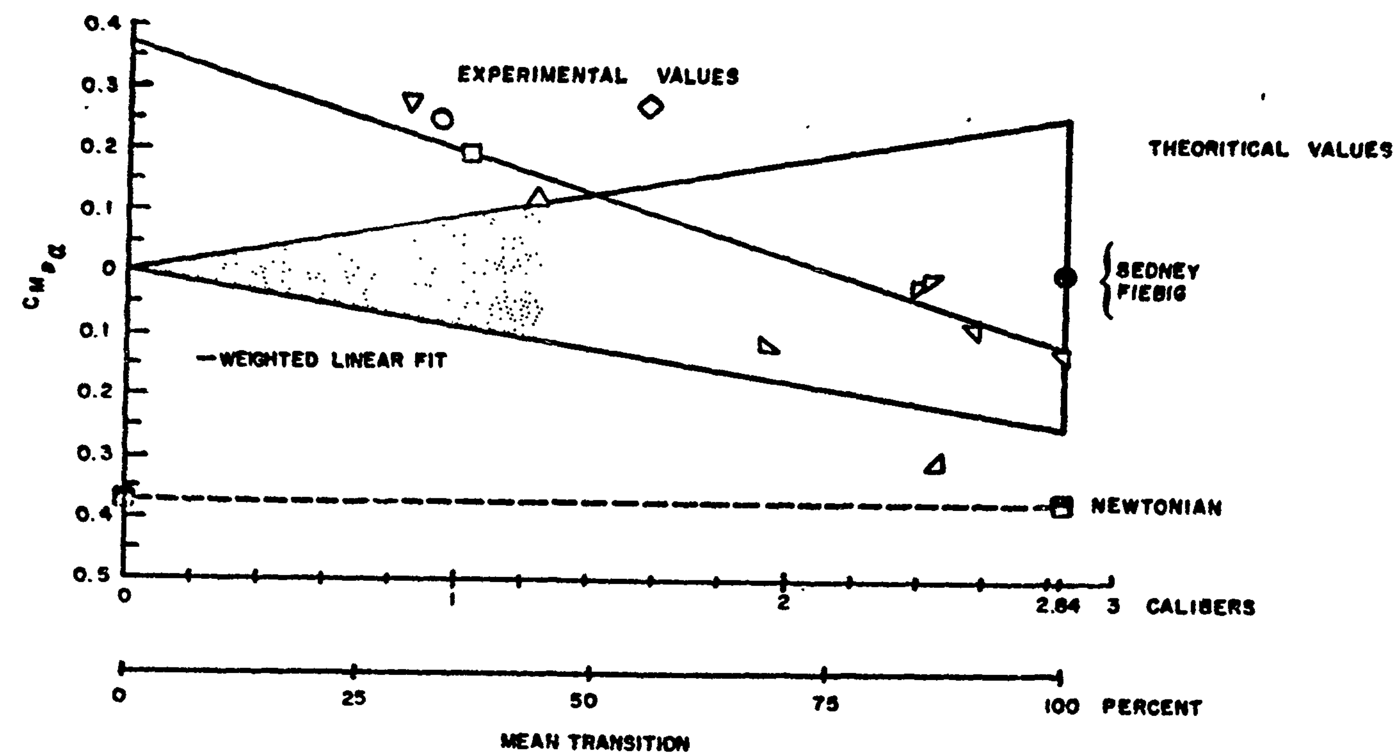

FIG 14 COMPARISON OF THEORITICAL AND EXPERIMENTAL VALUES OF $C_{M_{p\alpha}}$